# Bubble formation at a flexible orifice with liquid cross-flow

Karine Loubière, Vincent Castaignède, Gilles Hébrard, Michel Roustan

# BUBBLE FORMATION AT A FLEXIBLE ORIFICE WITH LIQUID CROSS-FLOW

**Karine Loubière, Vincent Castaignède, Gilles Hébrard (*), Michel Roustan**

*Laboratoire d'Ingénierie des Procédés de l'Environnement, Département G.P.I., INSA, 135 avenue de Rangueil, 31077 Toulouse Cedex 4, FRANCE*

**Abstract.**

In waste water treatment, biological processes for denitrification and nitrification are performed using oxidation ditches. In these reactors, the mixing and the aeration functions are dissociated: a bubble cloud is generated from flexible membrane spargers and is subjected to a horizontal liquid flow. The objective of this paper is to study the effects of the liquid cross-flow on the bubble formation at a single flexible orifice in water. The several forces acting on the forming bubble have been modelled in order to understand the dynamics of the bubble growth and detachment. The bubble detachment is controlled by the drag force due to the liquid motion and not by the buoyancy force. The experimental analysis of the bubble growth has shown that, under liquid cross-flow conditions, the bubbles move downstream and are flattened during their growth (position of the bubble centre of gravity, bubble inclination angle). The bubbles spread over the orifice surface, and the advancing and the receding bubble angles were measured. The detached bubbles have significantly smaller sizes and higher frequencies when compared to bubble formation under quiescent liquid conditions.

## 1. INTRODUCTION

For waste water treatment, biological processes for denitrification and nitrification are based on dissolved pollution consumption by micro-organisms. The oxygen necessary to the micro-organism metabolism is distributed in the tank by aeration systems. Whilst in chemical

(*) Corresponding author.Tel.:00 33 05 61 55 97 89; Fax:00 33 05 61 55 97 60; E-mail address: hebrard@insa-tlse.fr

industries the aeration is mainly performed with rigid nozzles (perforated plates or porous disk diffusers), a gas sparger based on a flexible membrane was developed for waste water treatment. A very uniform size distribution of small bubbles is achieved with this rubber punctured sheet: the gas hold-up and mass transfer area are significantly increased [1]. Moreover, it is found to be self-cleaning and does not suffer the usual clogging problems during the anaerobic period.

The aeration tanks used are mainly oxidation ditch type: their configuration is based on the dissociation between the mixing and the aeration functions, which enables the nitrogen removal to be increased. For this purpose, in addition to gas spargers, a horizontal liquid flow is generated inside the oxidation ditch by mixing systems (impellers localised at the surface or in the liquid medium). This horizontal liquid velocity modifies the global hydrodynamics of the ditch (elimination of spiral flows) and leads to an increase in the interfacial area and the mass transfer coefficient [2]. To understand these global results better, the present work intends to study the impact of the liquid cross-flow on the bubble generation at the gas sparger orifices. As the field offered by this topic is wide, our research is limited to the bubble formation at a single orifice submerged in water and under atmospheric conditions; only the dynamic bubbling regime is considered.

In many industrial gas-liquid operations, the continuous phase is caused to flow normally across the path of the emerging gas at the orifices. Thus, the bubble formation phenomenon under such conditions has been the subject of many experimental and theoretical studies [3-4]. The presence of a liquid cross-flow offers two major advantages [5]:

- Smaller bubbles are produced when compared to bubble formation under quiescent liquid conditions;
- The detached bubbles tend to be swept away from the region of the orifice, thereby reducing the likelihood of coalescence.

These studies are always based on the bubble generation at a rigid orifice, and there is a lack of research related to a flexible orifice (membrane sparger).

To fill this gap, the aim of this paper is to study the bubble formation at a flexible orifice under liquid cross-flow conditions. The several forces acting on the forming bubble will be modelled in order to understand the dynamics of the bubble growth and detachment under these operating conditions. Moreover, an experimental approach based on image analysis will be performed: it will allow the dynamics of the bubble formation and the detached bubbles to be characterised.

## 2. THEORETICAL APPROACH

Under quiescent liquid conditions, analytical models have been proposed to describe the bubble growth and detachment at a rigid orifice [3-4] and at a flexible orifice [6]; they lead to satisfactory and successful predictions, provided that the operating conditions agree with the model hypothesis. Under liquid cross-flow conditions, the dynamics of the bubble formation is more complex (velocity gradient, bubble inclination and distortion). Thus, the non-spherical models of bubble formation, which are the most currently used, become very difficult to adapt: doubtful assumptions have to be made and numerical instabilities are generated [5,7].

The aim of the present theoretical study is not to develop a complete model, but to understand the dynamics of the bubble growth and detachment at a flexible orifice under liquid cross-flow conditions. For this purpose, the horizontal and vertical components of the several forces acting on the forming bubble have to be calculated: the associated expressions are reported in Table 1.

The buoyancy and gas momentum forces have only vertical components, which are expressed in the same way as for quiescent liquid conditions [6,8]. The two components of the viscous drag force are deduced from [9]. Neglecting wall effects, the viscous drag coefficient $C_D$ is

deduced from the following equation [10]:

$$C_D = \frac{24}{Re_B}(1 + 0.15\,Re_B^{\,0.687}) \quad \text{for} \quad Re_B \le 1000$$
$$C_D = 0.44 \quad \text{si} \quad Re_B \ge 1000 \tag{9}$$

The associated Reynolds numbers are defined as [9]:

$$Re_{B,x} = \frac{\rho_L.(U_L - \frac{dx}{dt}).d_B}{\mu_L} \qquad Re_{B,y} = \frac{\rho_L.(\frac{dy}{dt}).d_B}{\mu_L} \tag{10}$$

The velocity $U_L$ in Eqs. (3) and (7) is equal to the mean velocity of the liquid flow: no velocity gradient is assumed in the vicinity of the forming bubble.

*Table 1. Several forces acting on the bubble under liquid-cross flow conditions*

| FORCE | HORIZONTAL COMPONENT | VERTICAL COMPONENT |
|---|---|---|
| BUOYANCY | - | $F_{B,y} = (\rho_L - \rho_G).g.V_B$ (1) |
| GAS MOMENTUM THROUGH THE ORIFICE | - | $F_{M,y} = \frac{4.\rho_G.(\frac{dV_B}{dt})^2}{\pi.d^2_{OR}}$ (2) |
| VISCOUS DRAG | $F_{D,x} = -\frac{1}{2}.\rho_L.(\frac{\pi.d_B^2}{4}).C_D \times(U_L - \frac{dx}{dt})^2$ (3) | $F_{D,y} = -\frac{1}{2}.\rho_L.(\frac{\pi.d_B^2}{4}).C_D.(\frac{dy}{dt})^2$ (4) |
| SURFACE TENSION | $F_{S,x} = -d_W.\sigma_L.\frac{\pi(\theta_A - \theta_R)}{\pi^2 - (\theta_A - \theta_R)^2} \times 1.25[\sin(\theta_A) + \sin(\theta_R)]$ (5) | $F_{S,y} = -d_W.\sigma_L.\frac{\pi}{(\theta_A - \theta_R)} \times[\cos(\theta_R) - \cos(\theta_A)]$ (6) |
| INERTIAL (ADDED MASS) | $F_{I,x} = C_I.\rho_L \times\left[(U_L - \frac{dx}{dt}).\frac{dV_B}{dt} - V_B.\frac{d^2x}{dt^2}\right]$ (7) | $F_{I,y} = -C_I.\rho_L \times\left[\frac{dy}{dt}.\frac{dV_B}{dt} + V_B.\frac{d^2y}{dt^2}\right]$ (8) |

The surface tension force is expressed as two components [11] and is a function of the liquid surface tension $\sigma_L$, the surface/bubble contact diameter $d_W$ and the bubble contact angles $\theta_A$ and $\theta_R$. The use of $d_W$ instead of $d_{OR}$ is essential in order to take into account the bubble spread over the orifice surface [6].

The two components of the inertial force [9] include the added mass coefficient $C_I$ which is taken as 11/16 [12,13]. The choice of 11/16 is certainly not ideal for a non-spherical growing bubble in contact with a wall and subjected to a liquid cross-flow, but no precise information concerning this particular case is available in the literature, so it was taken by default. The lift and the Basset forces are neglected in the present study.

## 3. MATERIAL AND METHODS

### 3.1 EXPERIMENTAL SET-UP

The 1 $m^3$ oxidation ditch of Simon et al. [14] is used for the experimental set-up. Figure 1 shows a schematic diagram of this pilot plant with its geometrical characteristics: it has an oblong geometry with outer and inner flow guides. The liquid phase circulation is performed with an axial impeller, type A310 marine propeller, 0.144 m in diameter, located at half liquid height. To minimise the liquid disturbances at the orifice, a high density polystyrene sheet is placed at the bottom of the ditch (2 m before the gas sparger) flush with the membrane sparger. The air flow rate is regulated by a pressure gauge and by a gas flow meter. The membrane sparger (60 mm diameter) is assembled on a circular clamping ring composed of two jaws; this fixing system coupled with the use of a dynamometric spanner (0 - 5 Nm) enables the same initial tension to be applied. The pressure drop created by the membrane is determined using an electronic manometer type Bioblock 915PM247. The bubbles are generated by a single puncture located at the membrane centre. The average gas flow rate $Q_G$ is measured using a soap film meter, through a funnel put on the clamp.

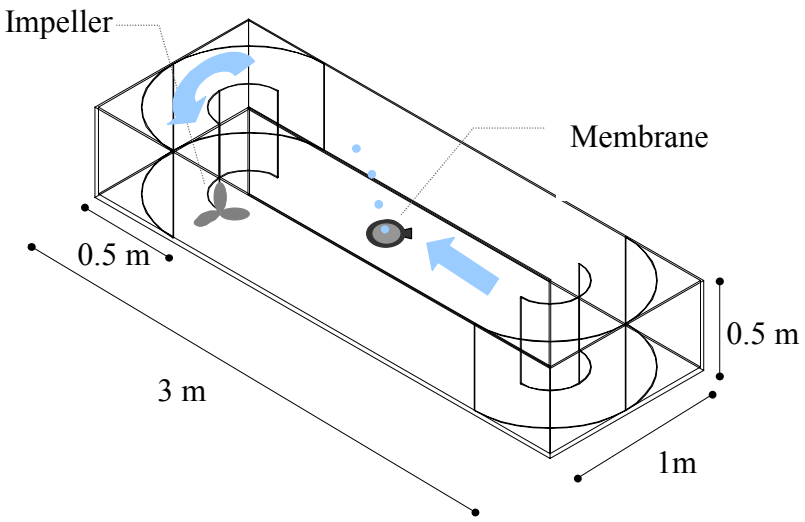


*Figure 1. Schematic diagram of the experimental set-up*

Water is used as the liquid phase, its physical properties are measured and are the following at the ambient temperature (around 20°C): $\rho_L$ = 997 kg/m$^3$, $\mu_L$ = 8.74×10$^{-4}$ Pa.s, $\sigma_L$ = 71.8 mN/m. All the measurements are performed at decreasing values of pressure (hysteresis phenomenon) [6].

*Table 2. Operating conditions*

| Flexible orifice | $H_L$ (m) | $d_{OR}$ (mm) | $Q_G$ (ml/s) | $U_{OR}$ (m/s) | $U_L$ (m/s) |
|---|---|---|---|---|---|
| M1 | 0.36 | 0.28 - 0.42 | 0.007 - 0.8 | 0.12 - 5.80 | 0.20 - 0.53 |
| M2 | 0.36 | 0.25 - 0.26 | 0.08 - 0.3 | 1.62 - 5.65 | 0.20 - 0.53 |

The operating conditions are reported in Table 2. Two rubber membranes are used as flexible orifices: an “housing” membrane called M1, and an industrial membrane called M2. They were characterised in terms of orifice diameter, wettability, elasticity and pressure drop. This characterisation showed that [6,15]:

- the M1 membrane is more elastic than the M2 membrane,
- for a given gas flow rate, the M1 orifice is larger than the M2 orifice and the M1 membrane creates larger pressure drop than the M2 membrane.

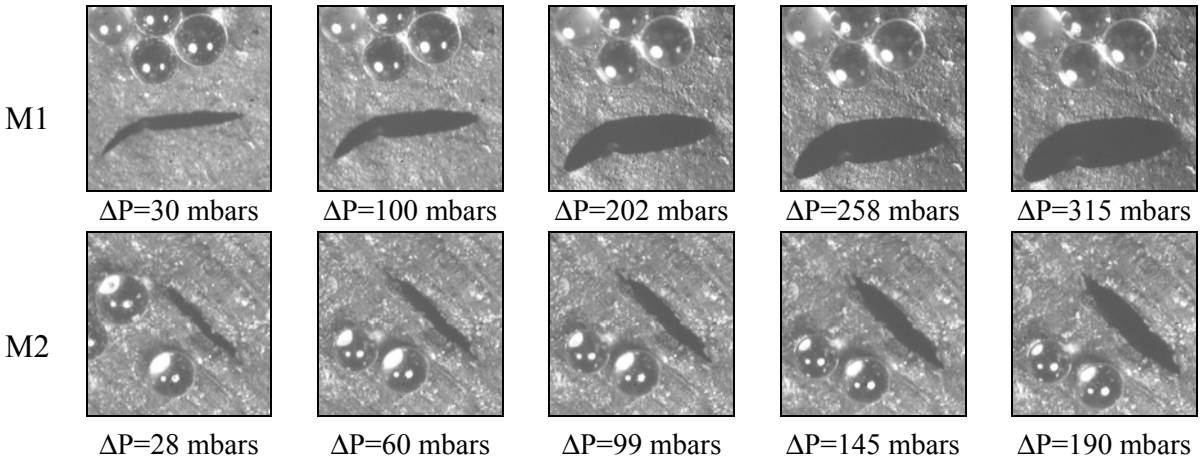


*Figure 2. Hole photographs (Calibration : glass particles 300 µm in diameter)*

It is important to bear in mind that when an increasing pressure is applied, owing to its elastic nature, the membrane bulges (shape of a spherical cap), the hole diameter expands and also varies in shape (Figure 2). Whatever the membranes, the hole appears as a slit: the eccentricity of the M1 and M2 holes varies between 9 and 4 for pressure drops below 200 mbars [15].

### 3.2 METHODS

*Image acquisition and treatment systems*

During their formation, bubbles are photographed with a Leutron LV95 camera (360 images/s). Images are visualised on the acquisition computer through the Leutron vision software. The Visilog 5.4 software performs the image treatment. The following parameters are determined: equivalent bubble diameter ($d_B$), centre of gravity co-ordinates (x,y), bubble contact angles ($\theta_A$, $\theta_R$) and surface/bubble contact diameter ($d_W$). The bubble frequency is deduced from photographic analysis.

*Liquid velocity measurements*

The liquid flow is measured using two methods: the micro-impeller technique and the ultrasound Doppler technique (Dop2000 probe) [15]. In both cases, the liquid flow around the generated bubbles is assumed to be uniform and thus a mean liquid velocity is considered.

The reality is somewhat more complex, as the liquid flow is affected by the ditch bottom and the membrane bulging; unfortunately, certain technical limitations prevent the liquid flow gradient in the vicinity of the forming bubbles being measured locally. The range of the mean liquid velocities studied is reported in Table 2.

## 4. RESULTS AND DISCUSSION

Only the results related to the M1 membrane will be detailed and introduced as follows:

- Firstly, the variations in the different parameters during the bubble growth will be presented, allowing the dynamics of the bubble growth to be described;
- Then, the detached bubbles will be characterised in terms of inclination angle, diameter and frequency;
- Lastly, the results related to the forces acting on the bubbles will be presented.

### 4.1 DYNAMICS OF THE BUBBLE GROWTH

*Visual observation*

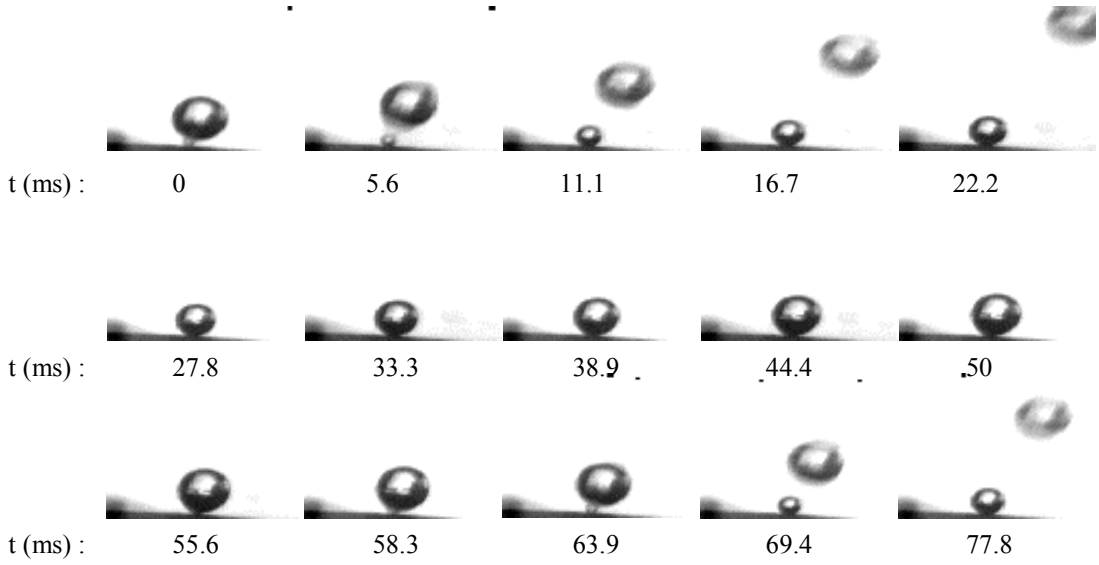


*Figure 3. Bubble formation at the flexible orifice under liquid cross-flow conditions ($d_{OR}$=0.32 mm, $U_{OR}$=0.50 m/s, $U_L$=0.20 m/s, $d_{B\ détachement}$=1.65 mm)*

Thanks to image analysis, the bubble generation process can be split up into different stages and so described experimentally. Figure 3 shows typical photographs of bubble generation from the flexible orifice under liquid cross-flow conditions. The bubble generation is composed of three stages: bubble growth ($0 < t < 58.3$ ms), bubble detachment ($t = 58.3$ ms) and bubble ascension ($t > 58.3$ ms).

*Bubble centre of gravity and bubble radius during growth*

Figure 4 illustrates a typical variation in the bubble centre of gravity co-ordinates and in the bubble radius with the growth time.

Unlike bubble formation under quiescent liquid conditions [6], the bubble centre of gravity abscissa x is not nil during the bubble growth, but increases linearly. Thus, the bubble growth is not symmetric about the vertical orifice axis; such a behaviour is characteristic of the horizontal bubble displacement under the influence of the liquid cross-flow.

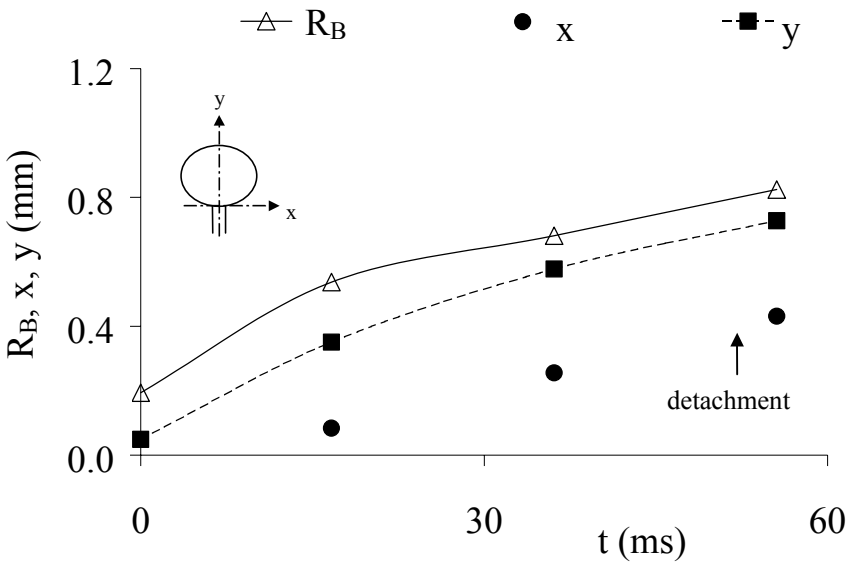


*Figure 4. Bubble radius and bubble centre of gravity co-ordinates versus growth time*

*($d_{OR}$=0.32 mm, $U_{OR}$=0.50 m/s, $U_L$=0.20 m/s, $d_{B\ détachement}$=1.65 mm)*

Whatever the growth time, the bubble centre of gravity ordinate y is less than the bubble

radius $R_B$. The bubble is not spherical but distorted, that is to say, flattened under the liquid velocity effect.

The experiments have shown that an increasing liquid velocity tends to intensify the downstream bubble motion and the bubble flattening.

*Bubble inclination during growth*

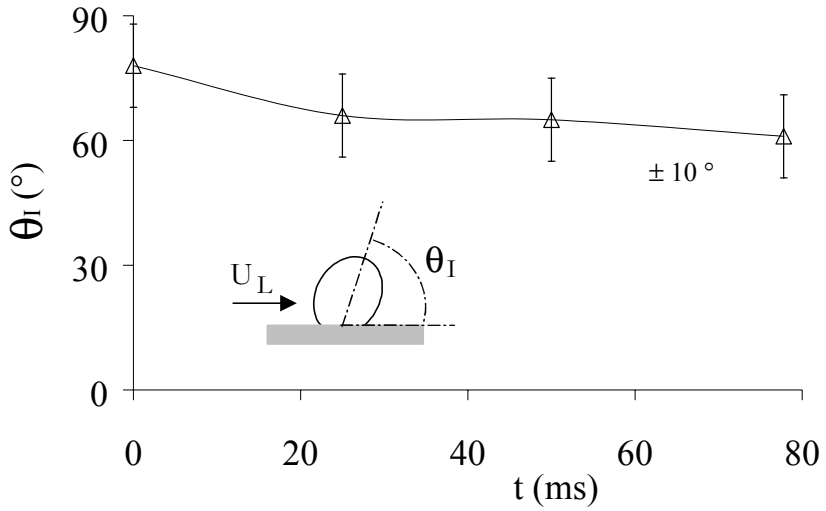


*Figure 5. Bubble inclination angle versus growth time ($U_L$=0.28 m/s, $U_{OR}$=0.12 m/s)*

The downstream bubble motion and its flattening have been highlighted previously (Figure 4). In order to characterise explicitly this phenomenon, some measurements of the bubble inclination angle $\theta_I$ were taken using image treatment. A typical variation in the bubble inclination angle with the growth time is plotted in Figure 5.

At the beginning of the bubble formation, the bubble inclination angle is near to 90°: the bubble is not yet subjected to the liquid velocity. Afterwards, the bubble inclination angle decreases continuously until levelling off: a minimum angle value is reached, remaining constant until the bubble detaches. Whatever the orifice gas velocities and the liquid velocities, the same tendency was observed.

*Bubble volume and gas flow rate supplying the bubble during growth*

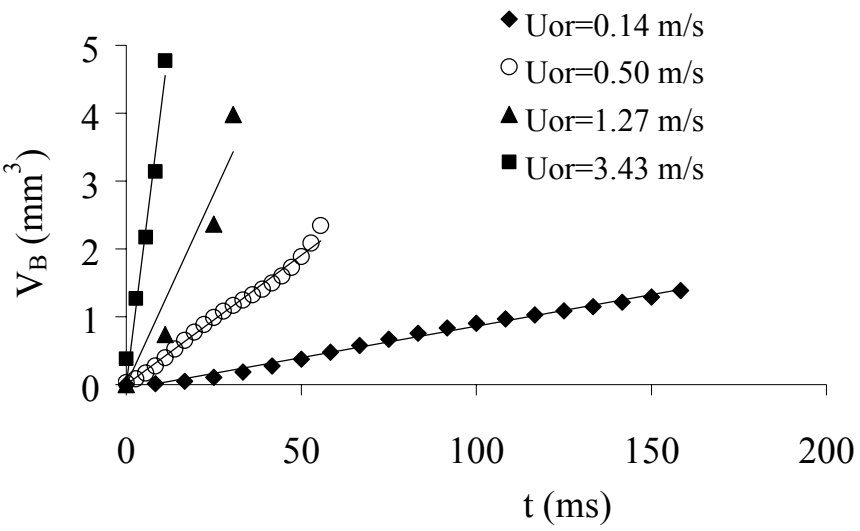


*Figure 6. Bubble volume versus growth time ($U_L$=0.20 m/s)*

Figure 6 presents some typical curves relating the bubble volume to the growth time. The bubble volume varies linearly with the growth time: this result remains valid whatever the orifice gas velocities and the liquid velocities. An increasing orifice gas velocity tends to increase the bubble volume and to decrease the bubble formation time.

The gas flow rate supplying the bubble q can be calculated by using the bubble volume values, as expressed:

$$q = \frac{dV_B}{dt} \qquad (11)$$

As the bubble volume varies linearly, the gas flow rate q remains constant during the bubble growth, and is equal to the mean gas flow rate $Q_{G,}$ whatever the orifice gas velocities and the liquid velocities.

Such behaviours of $V_B$ and q have already been observed under quiescent liquid conditions: they are specific to bubble formation at a flexible orifice [8].

*Continuity of the bubble formation*

The visualisation of the bubble formation (Figure 3) under liquid cross-flow conditions shows

that at the moment when a bubble detaches, a new bubble is growing, pushing off the previous one; no time-out exists between two bubbles formed successively at the flexible orifice. Unlike the bubble formation at a rigid orifice [8], the process is continuous: the bubble formation time is equal to the bubble growth time.

*Bubble adhesion to the orifice surface*

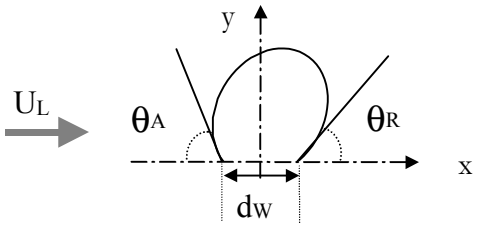


*Figure 7. Contact angles and surface/bubble contact diameter*

In order to shed light on the phenomenon of bubble adhesion to the orifice surface, the surface/bubble contact diameter $d_W$ and the bubble contact angles $\theta_A$ and $\theta_R$ were measured experimentally (Figure 7). Figure 8 presents typical variations in the ratio $d_W/d_{OR}$ with the growth time for different orifice gas velocities and liquid velocities. The orifice diameter used, $d_{OR}$, is an equivalent diameter, which corresponds to the diameter of the circular hole with the same area: they are measured by using a camera coupled to a microscope [6].

As shown in Figure 8, $d_W/d_{OR}$ remains mainly above 1: the bubble also spreads over the orifice surface. This can be explained by the hydrophobic nature of the orifice surface: its critical wettability surface tension $\gamma_C$ is equal to 23 mN/m [6]. Moreover, the variation in $d_W/d_{OR}$ with growth time is composed of two stages:

- the radial expansion stage, which is characterised by an increasing bubble spread,
- the elongation stage, which is characterised by a decreasing bubble spread.

The same tendency has already been observed under quiescent liquid flow [6,8].

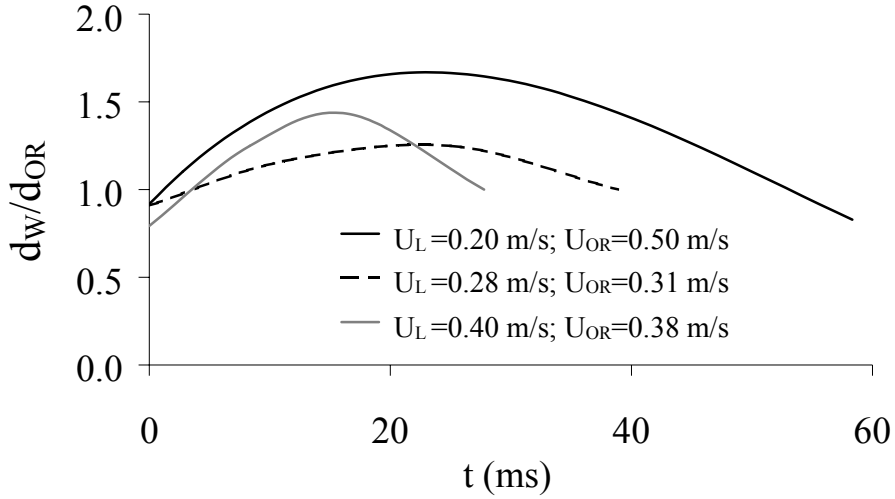


*Figure 8. Ratio of the surface/bubble contact diameter to the orifice diameter versus time*

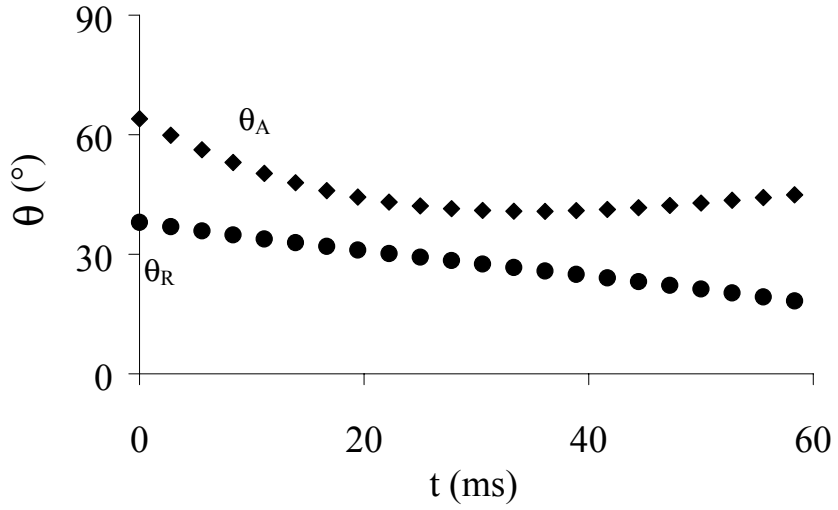


*Figure 9. Bubble contact angles versus growth time ($U_L$=0.20 m/s; $U_{OR}$=0.14 m/s)*

Figure 9 presents typical variations in the bubble contact angles $\theta_A$ and $\theta_R$ with the growth time. Whatever the orifice gas velocities and the liquid velocities, it can be observed that during the bubble growth:

- the advancing bubble contact angle $\theta_A$ is larger than the receding bubble contact angle $\theta_R$. The inequality between these two angles confirms that the bubble growth is not symmetric about the vertical orifice axis under such conditions;

- the advancing bubble contact angle $\theta_A$ decreases continuously as under quiescent liquid conditions [6,8];
- The receding bubble contact angle $\theta_R$ decreases linearly.

### 4.2 ANALYSIS OF THE DETACHED BUBBLES

The objectives of the present paragraph are to characterise the detached bubbles (inclination angle, diameter, frequency) as a function of the orifice gas velocities and the liquid velocities and to compare the results with the quiescent liquid conditions. It is essential to state that the orifice velocity $U_{OR}$ used in the figures is calculated as follows:

$$U_{OR} = \frac{Q_G}{\pi d_{OR}^2 / 4} \qquad (12)$$

*Inclination angle of the detached bubbles*

The previous paragraphs have shown that under liquid cross-flow conditions, the bubble moves downstream and is flattened during its growth. To make clear this phenomenon, the bubble inclination angle was measured during bubble growth (Figure 5): except for the first moments, it remains constant until the bubble detaches. In addition, the effects of the orifice gas velocity and of the liquid velocity on this inclination angle will be evaluated in this part.

Figure 10 presents the variation in the bubble inclination angle with the orifice gas velocity for different liquid velocities. An increasing liquid velocity tends to decrease the bubble inclination angle. Also, the bubble inclination angle decreases continuously with increasing orifice gas velocity until levelling off; above 2 m/s, the bubble inclination angle no longer depends on the orifice gas velocity. The variation in the bubble inclination angle above $U_{OR}$=2 m/s with the liquid velocity is plotted in Figure 11. In this figure, the results related to the M2 flexible orifice are also reported.

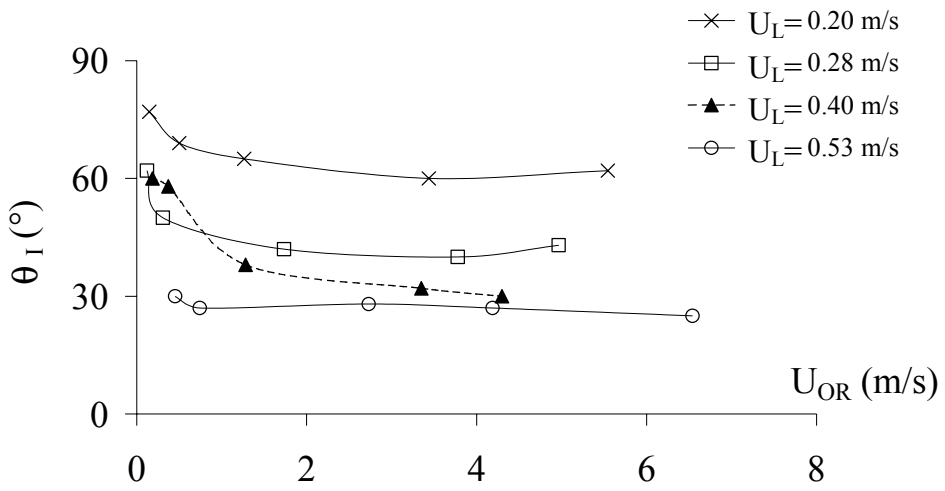


*Figure 10. Bubble inclination angle versus orifice gas velocity for different liquid velocities*

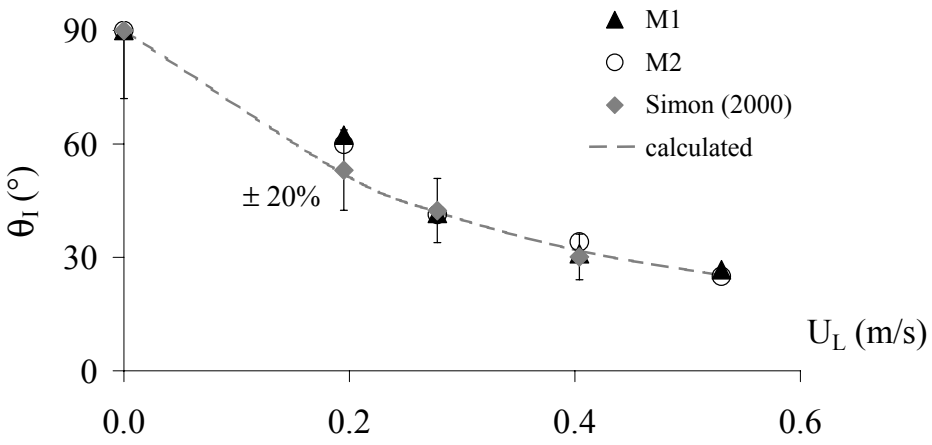


*Figure 11. Bubble inclination angle versus liquid velocity*

Figure 11 raises three comments:

- No significant difference exists between the inclination angles of the two orifices. Thus, for $U_{OR}$>2 m/s, the bubble inclination angle does not depend on the flexible orifice, but only on the liquid velocity.
- The global hydrodynamics and the mass transfer in our pilot plant (1 $m^3$ oxidation ditch) were studied by Simon (2000) [2]. In these studies, the average inclination angles of the bubble cloud generated from a multi-orifice membrane sparger were measured. Simon (2000) observed that these inclination angles of the bubble cloud don't depend on the gas flow rate, but only on the liquid velocity; their values are reported in Figure 11. They agree perfectly with the bubble inclination angle formed at

a single flexible orifice. Thus, whether the bubbles are generated from either a single flexible orifice or from a full membrane sparger, the bubble inclination angle remains roughly the same for a given mean liquid velocity. Due to the interactions between the bubble cloud and the liquid flow, the local hydrodynamic conditions above the sparger are different in both cases, but they have no significant consequences on the average bubble inclination angle. The bubble inclination angle is controlled only by the mean horizontal liquid velocity.

– Lastly, the bubble inclination angle can be roughly calculated by taking into account the bubble velocity $U_B$, its terminal rising velocity $U_t$ and the liquid velocity $U_L$ (Figure 12). The following equations are written:

$$U_B \approx \sqrt{(U_t)^2 + (U_L)^2} \tag{13}$$

$$\cos(\theta_I) \approx \frac{U_L}{U_B} \tag{14}$$

The bubble rising terminal velocity $U_t$ is around 0.25 m/s for bubble sizes between 1 and 2 mm [16]. For each liquid velocity, the bubble velocity $U_B$ is deduced from Eq.(13) and the bubble inclination angle $\theta_I$ from Eq.(14). Due to the experimental errors on $U_L$ and $U_t$, the calculated inclination angles are evaluated at ± 20%. These values are reported in Figure 11: a good agreement with the experimental bubble inclination angles is observed.

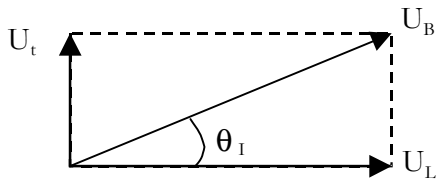


*Figure 12. Diagram allowing the bubble inclination angle to be calculated*

*Detached bubble diameter*

Figure 13 presents the curves relating the detached bubble diameter to the orifice gas velocity under quiescent liquid and liquid cross-flow conditions.

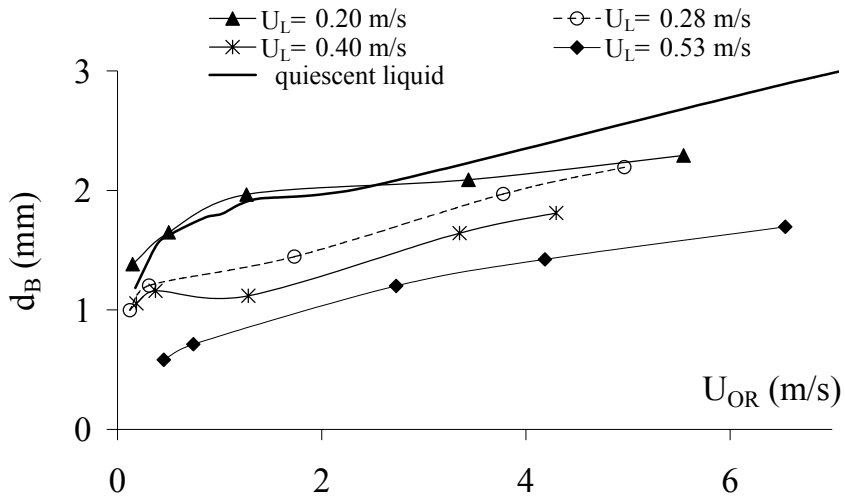


*Figure 13. Detached bubble diameter versus orifice gas velocity under quiescent liquid and liquid cross-flow conditions.*

Unlike the case of the rigid orifice [8], whatever the operating conditions, the bubble diameter increases logarithmically with the orifice gas velocity. Such a behaviour is specific to membrane spargers [6, 17]; this profile correlates to the orifice opening as increasing gas flow rate is applied.

Smaller bubbles are produced under liquid cross-flow conditions. For $U_L$=0.20, 0.28, 0.40 and 0.53 m/s, the bubble diameters are reduced to 10-15%, 20-40 %, 30-50% and 50-150 % respectively when compared to bubble formation under quiescent liquid conditions.

*Bubble frequency*

Figure 14 shows the variation in the bubble formation time with the orifice gas velocity under quiescent liquid and liquid cross-flow conditions.

Whatever the liquid velocity, the bubble formation time behaviour is the same as under quiescent liquid conditions. The bubble formation time decreases continuously with increasing orifice gas velocity until levelling off: above 2 m/s, $T_B$ remains roughly constant.

An increasing liquid velocity tends to decrease noticeably the bubble formation time. Under

the influence of the liquid velocity, the bubble frequencies are multiplied by a factor varying between 1.4 and 4.7 when compared to bubble formation under quiescent liquid conditions.

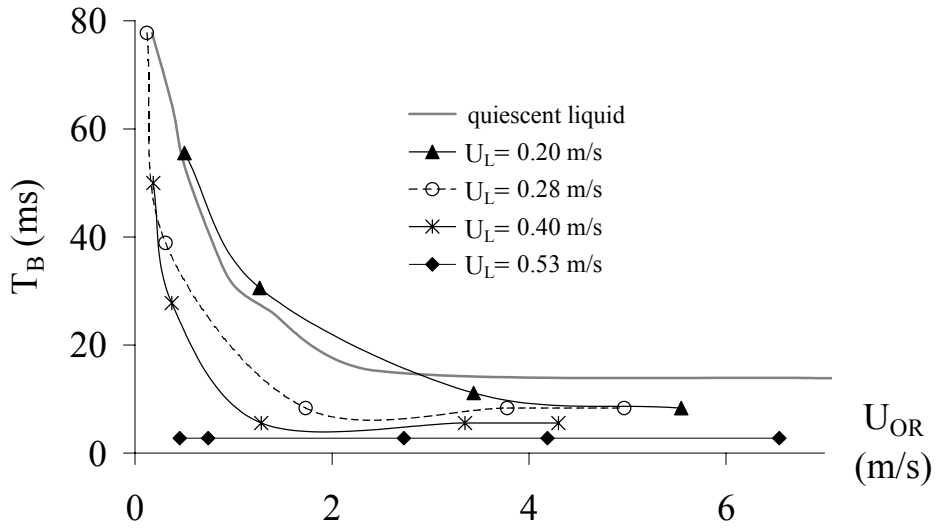


*Figure 14. Bubble formation time versus orifice gas velocity under quiescent liquid and liquid cross-flow conditions.*

### 4.3 FORCES ACTING ON THE BUBBLE DURING ITS GROWTH

The experimental data acquired are used to calculate the forces acting on the forming bubble (Table 1). Figure 15 (a) and (b) show typical variations in the horizontal and the vertical components of the forces with the growth time respectively.

(a)

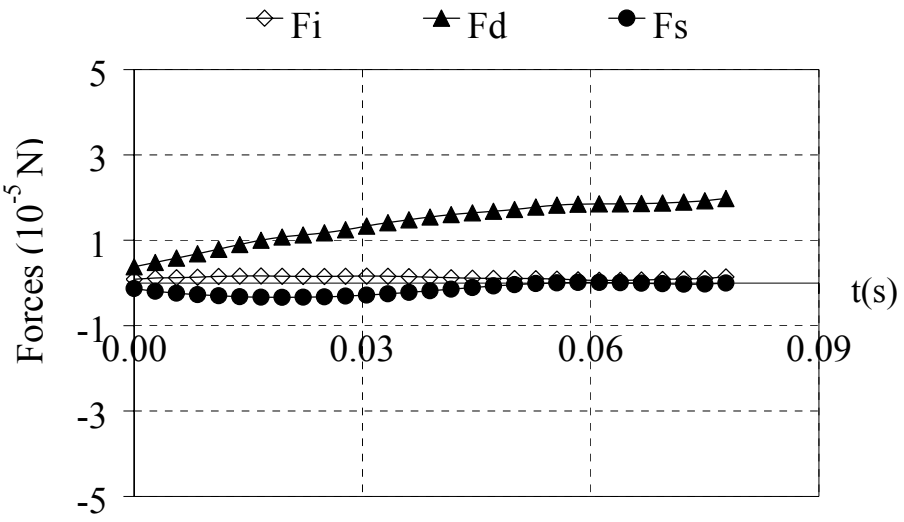

(b)

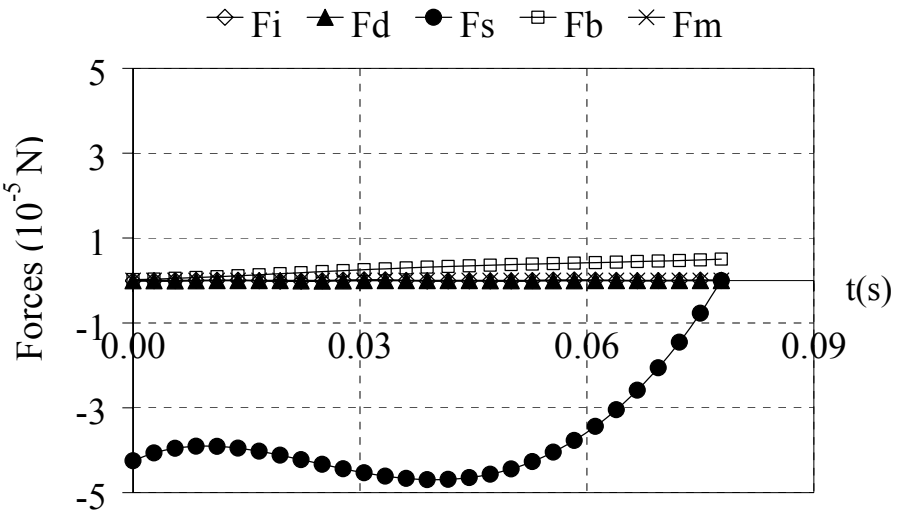


*Figure 15. Forces acting on the forming bubble versus growth time ($U_L$=0.28 m/s, $U_{OR}$=0.12 m/s). (a) Horizontal components (b) Vertical components.*

In the horizontal direction (x-axis), the drag force tends to detach the bubble whereas the surface tension force keeps the bubble attached to the orifice. The inertial force is not dominant.

In the vertical direction (y-axis), the bubble growth is governed by the buoyancy and the surface tension forces. The drag, inertial and gas momentum forces are negligible. The same tendency was observed under quiescent liquid conditions [6]. It is important to note that the vertical component of the surface tension force is significantly overestimated, which implies a force imbalance. The large experimental errors on $d_W$ (± 20 %) and on $\theta_A$ and $\theta_R$ (± 20°) can explain this result: the insufficient image definition in the vicinity of the orifice/bubble contact area prevents these parameters being determined precisely.

Comparison of the horizontal and vertical force components show that the horizontal component of the drag force is larger than the buoyancy force. Thus, it is the drag force due to the liquid cross-flow which is responsible for the bubble detachment and not the buoyancy force. This result is valid insofar as in our operating conditions, the liquid velocities are large

and the gas flow rates are small. The importance of the drag force is responsible for the previous results related to the dependence of the bubble inclination angle to the mean liquid velocity.

## 5. CONCLUSIONS

The objective of this research was to study the impact of the liquid cross-flow on the bubble generation at the gas sparger (rubber membrane) in oxidation ditches (waste water treatment). Because of the complexity of the phenomenon, only the bubble formation at a single orifice and the dynamic bubbling regime were studied. While most studies relate to bubbles generated at a rigid orifice (perforated plates or porous disk diffusers), the originality of this work was to consider a flexible orifice.

Under liquid cross-flow conditions, the dynamics of the bubble growth has been analysed and has shown that:

- during its growth, the bubble moves downstream and is flattened due to effect of the liquid motion;
- except for the first moments, the bubble inclination angle remains roughly constant during the bubble growth; it depends only on the liquid velocity and can be calculated;
- as under quiescent liquid conditions [6], the bubble volume varies linearly with the growth time;
- the bubble formation at a flexible orifice remains a continuous phenomenon;
- as under quiescent liquid conditions [6], the bubble spreads over the orifice surface during its growth; the bubble advancing contact angle is larger than the receding one;
- the force which is responsible for the bubble detachment is the drag force due to the liquid cross-flow and not the buoyancy force.

This study has clearly proved that the liquid velocity has a strong impact on the bubble

generation at the gas sparger orifices: the bubbles formed have significantly smaller sizes and higher formation frequencies, when compared to bubble formation under quiescent liquid conditions. Such results will have important consequences on gas hold-up, interfacial area and mass transfer in the reactor. In addition to the impact on the bubble generation, it is evident that the liquid velocity will modify the bubble coalescence and the likelihood of breakage during their ascent in the reactor, and the liquid mass transfer coefficient $k_L$. These points have to be analysed in detail in the future.

## NOTATION

*Roman symbols*

| | | |
|---|---|---|
| $d_{OR}$ | Equivalent orifice diameter | [m] |
| $d_W$ | Surface/bubble contact diameter | [m] |
| g | Acceleration due to gravity | [m/s$^2$] |
| $H_L$ | Liquid height in the oxidation ditch | [m] |
| $\Delta P$ | Pressure drop created by the membrane sparger | [Pa] |
| $Q_G$ | Mean gas flow rate (measured with the soap film meter) | [m$^3$/s] |
| $U_L$ | Mean liquid velocity | [m/s] |
| $T_B$ | Bubble formation time | [s] |
| $V_B$ | Bubble volume | [m$^3$] |
| x | Bubble centre of gravity abscissa | [m] |
| y | Bubble centre of gravity ordinate | [m] |

*Greek symbols*

| | | |
|---|---|---|
| $\gamma_C$ | Wetting critical surface tension of the orifice surface | [N/m] |
| $\theta_A$ | Advancing contact angle between the bubble and the orifice surface | [°] |
| $\theta_I$ | Bubble inclination angle | [°] |
| $\theta_R$ | Receding contact angle between the bubble and the orifice surface | [°] |
| $\mu_L$ | Liquid viscosity | [Pa.s] |
| $\rho_G$ | Gas density | [kg/m$^3$] |
| $\rho_L$ | Liquid density | [kg/m$^3$] |
| $\sigma_L$ | Liquid surface tension | [N/m] |

## REFERENCES


[1] Rice R.G., Tupperainen J.M.I., Dispersion and gas hold up in bubble columns. Comparison of rigid and flexible spargers, Can. J. Chem. Eng. 59 (1981) 677.

[2] Simon S., Etude d'un chenal d'oxydation par des approches globales et locales.

Hydrodynamique et transfert de matière, Thèse N°582 INSA Toulouse France (2000).

[3] Tsuge H. Hydrodynamics of bubble formation from submerged orifice. Encyclopaedia of Fluid Mechanics, Edited by Cheremisinoff Gulf Publishing Corporation Houston TX 43 Chap. 9 (1986)191-232.

[4] Sadhal S.S., Ayyaswany P.S., & Chuang J.N., Transport Phenomena with Drops and Bubbles, Springer Verlag, New York (1997).

[5] Tan R.B.H., Chen W.B., Tan K.H., A non-spherical model for bubble formation with liquid cross-flow, Chem. Eng. Sc. 55 (2000) 6259-6267.

[6] Loubière K., Hébrard G., Bubble formation from a flexible hole submerged in an inviscid liquids, Chem. Eng. Sc. 58 1 (2003) 135-148.

[7] Zhi Li H., Du simple vers le complexe: une nouvelle approche des fluides non newtoniens, Habilitation à diriger des recherches, Institut National Polytechnique de Lorraine (1998).

[8] Loubière K., Hébrard G., Guiraud P., Dynamics of bubble growth and detachment from rigid and flexible orifices, Can. J. Chem. Eng. subjected to publication as part of the 6th International Conference on Gas-Liquid and Gas-Liquid-Solid Reactor Engineering Vancouver Canada August 17-20 (2003).

[9] Colin C., Duhar G., Illa S., Croissance et Détachement de bulles dans un écoulement cisaillé, Proc. of Thermic French Conference (SFT) in Lyon (2000).

[10] Schiller L., Nauman A., A drag coefficient correlation, V.D.I. Zeitung 77 (1935) 318-320.

[11] Klausner J.F., Mei R., Bernhard D.M., Zeng L.Z., Vapor bubble departure in forced convection boiling, Int. J. Heat Mass Transfer 36 3 (1993) 651-662.

[12] Terasaka K., Tsuge H., Bubble Formation at a single orifice in highly viscous liquids, J. Chem. Eng. Jap. 23 (1990) 160-165.

[13] Milne-Thomson L.N., Theoretical Hydrodynamics, London : MacMillan & Co Ltd. 3rd edition (1955).

[14] Simon S., Roustan M., Audic J.M., Chatellier P., Prediction of mean circulation velocity in oxidation ditch, Env. Tech. 22 (2001) 195-204.

[15] Loubière K., Croissance et détachement de bulles générées par des orifices rigides et flexibles dans des phases liquids newtoniennes: Etude expérimentale and modélisation,Thèse N°663 INSA Toulouse France (2002).

[16] Grace J.R., Wairegi T., Properties and characteristics of drops and bubbles, Encyclopedia of Fluid Mechanics Cheremisinoff Chap. 3 Gulf Publishing Corporation Houston TX (1986) 43-57.

[17] Hébrard G., Bastoul D., Roustan M., Influence of the gas sparger on the hydrodynamic behaviour of bubble columns, Trans IchemE 74 A (1996) 406-414.